Transverse mechanical properties of carbon nanotube crystals. Part II: sensitivity to lattice distortions

E. Saether*

NASA Langley Research Center, MS 240, Hampton, VA 23681, USA

Abstract

Perfect crystals of carbon nanotubes tend to form aligned bundles that assume a hexagonal packing configuration in a minimum energy state. The theoretical constitutive relation for these defect-free crystals is highly anisotropic with a large axial stiffness due to a network of strong delocalized carbon–carbon bonds and transverse properties that are orders of magnitude lower due to a sole dependence on non-bonding van der Waals forces. The assemblage of a large number of collimated nanotubes may be expected to exhibit a distribution of lattice sites containing imperfections caused by packing faults or inclusions that will function as 'weak-links' and adversely affect local stiffness and strength. The present study is therefore directed towards quantifying the effects of distorted bundle configurations on mechanical properties. To illustrate distortion sensitivity, the transverse shear and bulk moduli are calculated by considering various magnitudes of random perturbations in nanotube packing. Monte Carlo simulations are performed to obtain a statistical distribution of predicted moduli. The present analysis demonstrates that even small perturbations to the lattice geometry give rise to large variations in transverse moduli, and suggests that chemical functionalization to improve nanotube bundle cohesion may be required for successful structural applications.
© 2003 Elsevier Science Ltd. All rights reserved.

Keywords: B. Mechanical properties; Carbon nanotubes; Bundles; Composites; C. Probabilistic methods

1. Introduction

Reported analytical predictions and experimental measurements of individual carbon nanotube axial moduli vary widely in the literature. This variation is primarily due to the assumed cross-sectional geometry of the nanotube used to define local continuum properties such as elastic moduli and moments of inertia for stiffness calculations. Using a cylindrical shell representation for an individual nanotube, the effective axial modulus is calculated to be on the order of 1.0 TPa [1,2]. Although the axial stiffness of individual nanotubes has been studied extensively, the determination of mechanical properties in the transverse plane of bundle configurations normal to the nanotube axes has not been adequately explored. The transverse properties are solely dependent on weak van der Waals forces that characterize the interactions between nanotubes. These forces cohesively bind the bundle and are the only mechanism through which loads can be transferred between individual nanotubes. A carbon nanotube bundle may be formally classified as a van der Waals solid and is highly anisotropic with constitutive properties that differ by orders of magnitude between the axial and transverse directions.

Techniques for carbon nanotube synthesis and processing are constantly evolving, yielding greater control of nanotube generation and manipulation. However, fabrication of microfilamentary assemblages consisting of huge numbers of collimated nanotubes is expected to result in bundles or ropes containing a distribution of various imperfections. These imperfections may include discontinuous nanotubes along the axis of the filament and cross-section lattice distortions, each causing significant reductions in stiffness and strength compared to a theoretical perfect bundle structure. Discontinuous nanotubes require that load carried by the covalent bonds in one nanotube be transferred to surrounding nanotubes through shear which is mediated by weak van der Waals forces. This mechanism of load transfer causes relative sliding of bundle nanotubes yielding

* Tel.: +1-757-864-8079; fax: +1-757-864-8912.
  E-mail address: e.saether@larc.nasa.gov (E. Saether).

reduced axial stiffness. Cross-sectional lattice distortions similarly cause a significant degradation in local transverse properties due to the extreme nonlinearity of the van der Waals interactions.

Distortions in the transverse lattice plane may be caused by various defects including embedded amorphous carbon, interspersed polymer from the surrounding media, Stone–Wales or pentagon–heptagon (5/7) defects in the bond structure of nanotube surfaces [3], local twisting or entanglement of nanotubes, and packing defects in the form of voids or deviations from a minimum energy hexagonal positional configuration. For example, Fig. 1 shows a cross section of a small nanotube bundle obtained from transmission electron microscopy (TEM). Although a precise interpretation of the image is difficult, some local regions appear to be fully populated yet deviate from a perfect hexagonal packing configuration while others appear to have missing nanotubes forming either voids or regions infused with amorphous material.

A recent concept for nanotube-based microfilaments has postulated a complex filamentary structure composed of ascending orders of bundle aggregates as shown in Fig. 2 [5]. It appears appropriate to assume that at each level of assembled bundle complexes, the
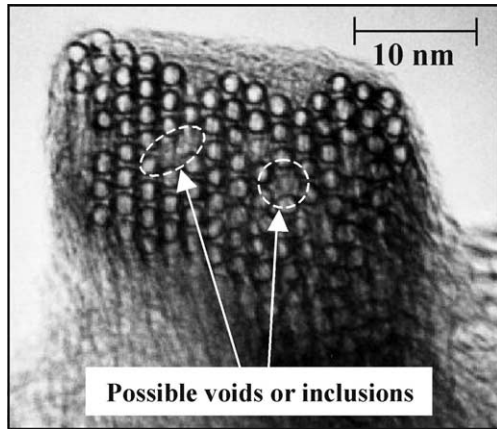
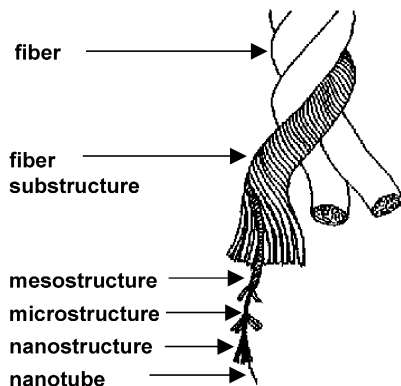

Fig. 1. Imperfect nanotube bundle [4].

Fig. 2. Structure of nanotube fiber.

hierarchical lattice will assume increasing levels of disorder. The physics of individual bundles at the nanoscale will ultimately dictate the effective higher-order continuum properties.

In this paper, the sensitivity of transverse mechanical properties to lattice distortions of carbon nanotube crystal lattices is examined. The following sections describe the calculation of transverse moduli together with details of a specific unit cell model used to simulate the nanotube lattice. Various assumptions employed to simplify the analysis are then discussed. Finally, a series of Monte Carlo simulations that quantify the sensitivity of transverse shear (G_{23}) and bulk moduli (K_{23}) to lattice distortions of varying magnitudes is presented followed by concluding remarks regarding the implications of the present analysis.

2. Calculation of transverse nanotube bundle moduli

A specialized methodology, presented in a companion paper [6], is utilized for calculating effective transverse moduli of nanotube bundles. In this approach, a unit cell model incorporating periodic boundary conditions is defined and specific strain modes applied. The kinematics of the shear and bulk strain modes used to calculate the G_{23} and K_{23} transverse moduli of a hexagonal nanotube bundle is shown in Figs. 3 and 4. The kinematic fields indicate the motion of the nanotube centroids from an initial stress-free position (x_{2o}, x_{3o}) under the applied strain. The dashed lines highlight the distortion of a unit hexagonal cell with surrounding image nanotubes in transforming from an unstrained to a deformed state. For shear straining, the magnitude of the strain is denoted by θ which corresponds to the developed shear angle. For bulk strain, the magnitude of the strain is given by e where $e = \varepsilon_{22} + \varepsilon_{33}$. The equal contributions of straining in the x_2 and x_3 directions give rise to a dilatational or volumetric strain mode.

The Lennard–Jones potential is used to compute the potential energy of nanotube interactions as a combination of repulsion caused by Pauli exclusion in π-cloud overlap and attraction due to instantaneously induced dipoles. The '6–12' form of this atom-pair potential is expressed as

$$\Phi_{o} = 4\varepsilon_{LJ}\left[\left(\frac{\sigma_{LJ}}{r_{ij}}\right)^{12} - \left(\frac{\sigma_{LJ}}{r_{ij}}\right)^{6}\right] \tag{1}$$

where ε_{LJ} is the depth of the energy well, σ_{LJ} is the van der Waals radius, and r_{ij} is the separation distance between the ith and jth atoms [7,8].

Effective initial elastic moduli are calculated from the change in potential energy due to imposed strain deformations as
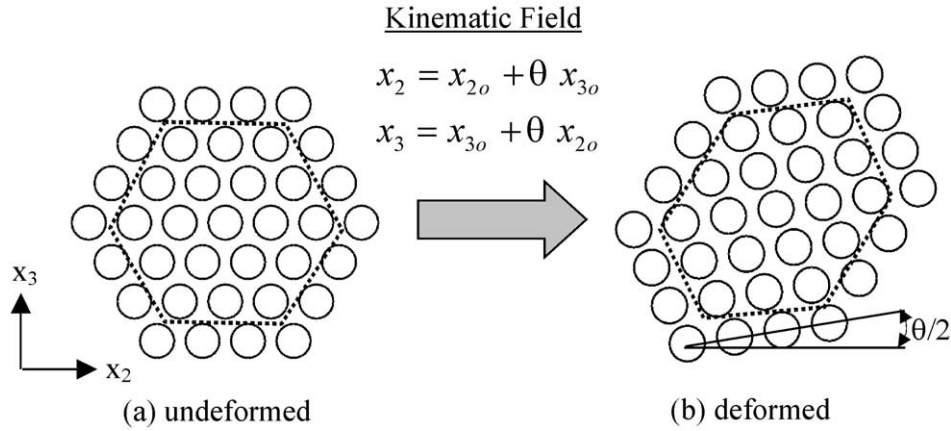
Kinematic Field

$$x_2 = x_{2o} + \theta\, x_{3o}$$
$$x_3 = x_{3o} + \theta\, x_{2o}$$

(a) undeformed (b) deformed

Fig. 3. Imposed transverse shear stain on hexagonally packed nanotube array.

Kinematic Field

$$x_2 = x_{2o} + e\, x_{2o}$$
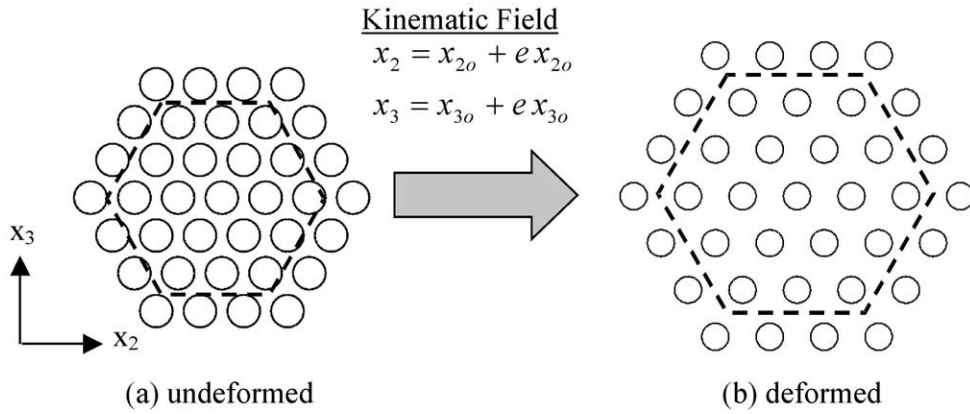$$x_3 = x_{3o} + e\, x_{3o}$$

(a) undeformed (b) deformed

Fig. 4. Imposed dilatational strain on hexagonally packed nanotube array.

$$C_{ij} = \frac{\partial^2 \Phi_o}{\partial \varepsilon_i \partial \varepsilon_j}. \qquad (2)$$

where C_{ij} is the material stiffness, Φ_o is the strain energy density, and ε_k is the applied strain mode. The strain modes are applied incrementally, and the potential energy calculated at each increment. The associated modulus is then obtained from Eq. (2) where the second derivative is computed numerically.

It is important to note that the Lennard–Jones pair potential may severely underpredict interaction forces in certain nanotube bundle straining modes. This potential assumes a spherical model of atoms in which the attractive force of induced dipoles is incorporated through an effective van der Waals radius and is solely a function of the radial separation distance, r_{ij}, of the atom centers. Straining in the transverse plane involves mostly relative radial motion of surface carbon atoms on adjacent nanotubes as shown in Fig. 5a and justifies the use of the Lennard–Jones potential. However, the van der Waals effects are not properly represented in shearing modes that involve relative tangential motion of atom pairs such as in axial sliding of adjacent nanotubes. As depicted in Fig. 5a, infinitesimal tangential motion

yields a nearly zero change in the separation distance, Δr_{ij}, which makes the Lennard–Jones estimate of the potential energy effectively independent of the motion. This issue has been studied for graphite [9,10] which has a delocalized electronic structure nearly identical to the electron orbital fields on the surface of carbon nanotubes. In these studies, the use of the Lennard–Jones potential has been shown to underpredict the modulus associated with parallel plane sliding by an order of magnitude.

3. Unit cell definition

Fig. 6 shows the unit cell used in the present analysis. A basic tileable unit of a hexagonally packed bundle is represented by three nanotubes labeled *A, B* and *C* in Fig. 6a. This triad is used to create a rhombic configuration by reflecting the orientation of nanotube *B* across a line joining the centers of nanotubes *A* and *C* and is denoted by B^{-1} as shown in Fig. 6b. The resulting rhombic unit cell is completed by the imposition of periodic boundary conditions, which establish the interaction of image nanotubes in surrounding cells, thereby simulating bundles of arbitrary size.
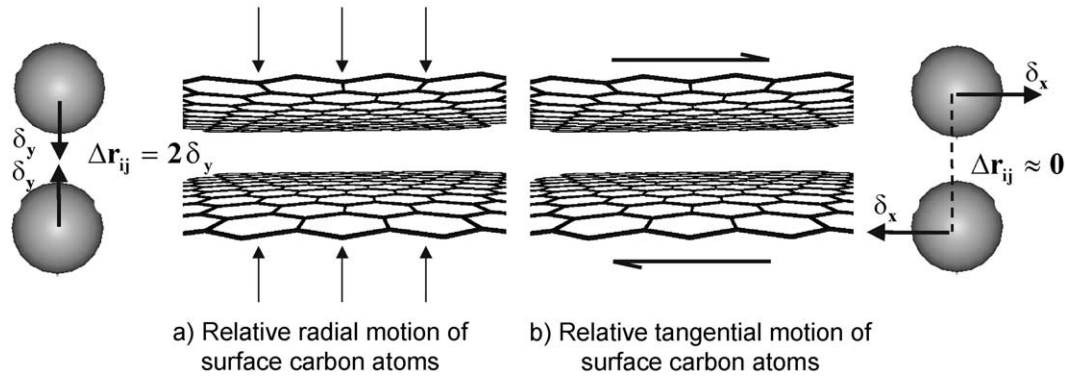
a) Relative radial motion of surface carbon atoms

b) Relative tangential motion of surface carbon atoms

Fig. 5. Relative motion of surface atoms on adjacent nanotubes.

a) Basic triangular unit
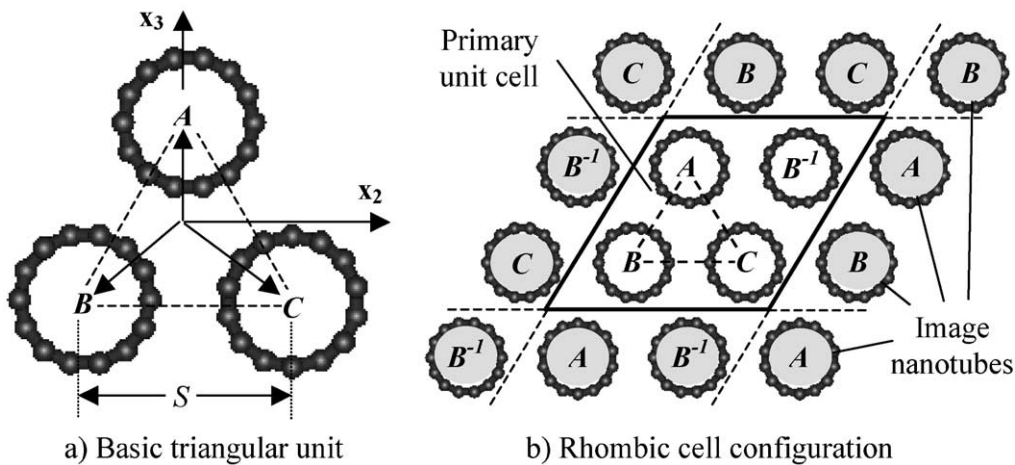
b) Rhombic cell configuration

Fig. 6. Unit cell configuration with periodic boundary conditions.

For the nanotube crystal used in the present study, all nanotubes were assumed to be single-walled and of equal diameter with an achiral zig-zag (12,0) conformation. Using a carbon–carbon bond length of 1.42 Å yielded nanotubes with a radius of 0.471 nm [11]. Nanotubes of this radius may be considered effectively rigid in the transverse plane [11–13]. Therefore, the only degree of freedom included in the deformations is the relative motion of the nanotube center. Equilibrating the system at 0 K resulted in an equilibrium nanotube center-to-center separation distance, S, of 1.26 nm. In the transverse plane, all cohesive forces generated during applied strain are due to van der Waals effects and modeled using the Lennard–Jones potential. The parameters used in the Lennard–Jones potential are $\varepsilon_{LJ} = 34.0$ K and $\sigma_{LJ} = 0.3406$ nm [11].

4. Analysis assumptions

Because of the wide range of possible defects that could conceivably occur in nanotube bundles, various simplifying assumptions have been made to demonstrate lattice distortion sensitivity in a very general manner. These assumptions are briefly discussed in the following subsections.

4.1. Reference nanotube bundle configuration

The material model of a carbon nanotube bundle in a reference minimum energy state, is assumed as a crystal consisting of a collimated array of straight nanotubes which exhibit a perfect hexagonal packing configuration in the cross-section. Because only defects in the transverse plane are considered and the nanotubes are assumed rigid, no elastic coupling with axial deformations occurs, yielding an effectively two-dimensional analysis.

4.2. Spatial distribution of lattice distortion

The model used in the present study assumes a uniform distribution of lattice distortion. In an actual bundle it may be assumed that large sections of the bundle cross-section would exhibit a perfect hexagonal packing configuration with a distribution of local sites containing defects. Therefore, the results of the current analysis must be regarded as a measure of effective

mechanical properties valid only in local regions exhibiting an assumed distortion in the lattice.

4.3. Initial equilibrium of the lattice

The current analysis models the mechanical properties associated with two-dimensional transverse planes along the nanotube bundle axis. Distortions are introduced into the transverse plane by repositioning nanotubes within a unit cell resulting in a non-equilibrium system. This situation occurs for packing faults that cause voids or non-hexagonal packing configurations, and also for instantaneous states due to thermal motion. However, for assumed polymeric or amorphous inclusions, the model used in the current study may be regarded as representing the bundle cross-section along the bundle axis in the near vicinity of the inclusion and not at the actual inclusion site. At the location of the inclusion, the system would be expected to equilibrate to a minimum energy state involving complex interactions with the atoms forming the inclusion. The detailed modeling of such nanotube-inclusion aggregates and the requisite equilibration is not attempted in the current study.

4.4. Thermodynamic state

The present analysis is focused on obtaining material moduli—which are continuum quantities—based on the energetics of discrete atomic interactions. In applying distortions to the assumed unit cell, relationships involving continuum thermodynamic variables of the atomic aggregate become important. These quantities are the number of particles, volume, temperature, and pressure denoted by N, V, T, and P, respectively. The use of the model developed in the companion paper [6] assumes a constant NVT thermodynamic system in which the temperature may be considered at 0 K. Introducing lattice distortions by repositioning nanotubes yields a sequence of non-equilibrium configurations that may be considered equivalent to thermal fluctuations. These distortions suggest that a constant NPT isobaric-isothermal state may be more appropriate. However, the present analysis maintains a constant volume constraint to define elastic moduli which violates an NVT state by making the effective temperature or pressure variable. Thus, increasing the magnitude of distortion to the lattice can be viewed as subjecting the system to an increase in pressure that will influence results. This influence is assumed not to significantly affect the demonstration of sensitivity in predicted moduli to lattice distortion.

5. Monte-Carlo simulation of lattice defects

Monte-Carlo simulations were used to analyze distortions by introducing random imperfections into the nanotube lattice from which effective elastic moduli were calculated. A distortion magnitude, δ, and direction, ϕ, were chosen as random variables to define perturbation vectors used to reposition the primary nanotubes A, B, and C, as shown in Fig. 7. In performing simulations, a maximum value for the distortion parameter was defined and intermediate values were randomly selected within the range $\delta \in (0, \delta_{max})$ for each trial. The directions were randomly selected within the angular range $\phi \in (0, 2\pi)$. Examples of distorted lattices, shown magnified by a factor of 150 for clarity, are presented in Fig. 8, and may be compared to the perfect lattice shown in Fig. 6. Imposing selected strain modes and calculating the infinitesimal change in potential energy, the bundle moduli were then obtained from Eq. (2).

Fig. 9 shows a coarse-binned relative histogram illustrating the distribution of the change in the center-to-center nanotube separation distance, ΔS, from a perfect lattice. This distribution for ΔS corresponds to a distortion magnitude $\delta_{max} = 0.125$ Å, and demonstrates that a uniformly random repositioning of the nanotubes yields a normal distribution with a zero mean and a standard deviation of 0.0712 Å.

For the present analysis, the distribution of the random perturbation variables were considered uniform implying that all values within selected ranges were assumed equally probable. The repositioning of the nanotubes within the unit cell generally results in a non-equilibrium cell configuration which is assumed to represent a locally distorted lattice at a particular cross-sectional location along the bundle axis. At the location of a void, this state would be considered representative of a bundle cross-section in which elevated distortion energy exists compared to the minimum potential energy of a perfect hexagonal packing configuration. At the location of the amorphous or polymeric inclusion, the bundle is distorted but naturally assumes an equilibrium energy state. However, along the bundle axis in the vicinity of this inclusion site, away from any electrostatic
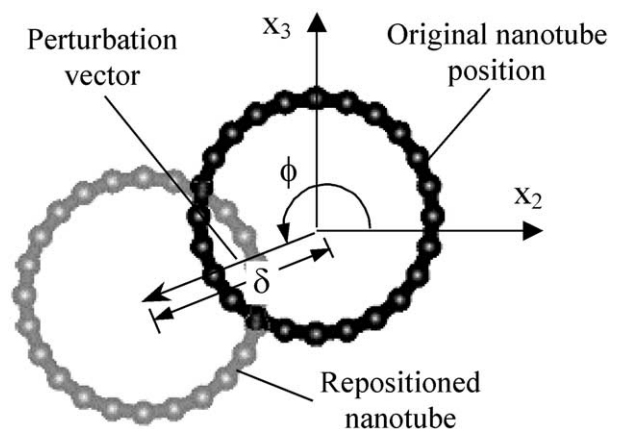

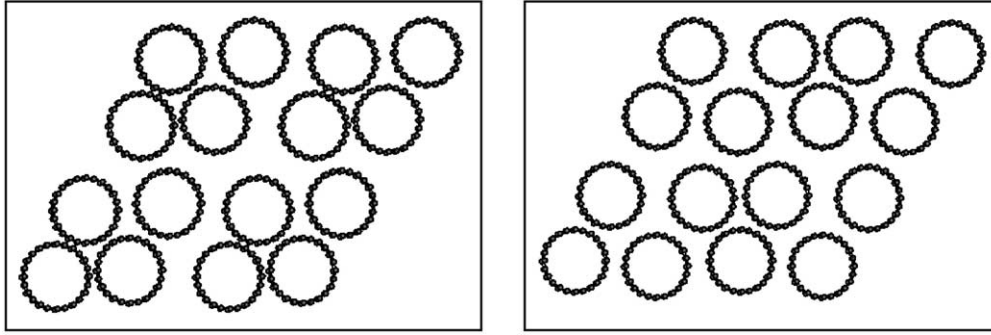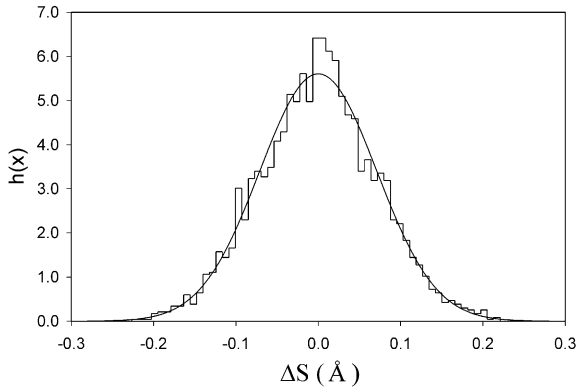Fig. 7. Nanotube repositioning in Monte-Carlo simulation.

Fig. 8. Examples of distorted lattice configurations (magnified for clarity).

Fig. 9. Distribution of nanotube separation ΔS for $\delta_{max} = 0.125$ Å.

interactions with the assumed inclusion and before the bundle resumes an undisturbed configuration, the lattice cross-section should exhibit a higher, non-equilibrium potential energy state and be effectively represented by the current distortion model.

The basic statistics of the computed moduli are given by the expectation or mean value, μ, and the standard deviation, σ. Due to the assumption of rigid nanotubes, the position of the system is defined by six degrees of freedom representing the two inplane translational components of the three primary nanotubes shown in Fig. 6a. Therefore, the required number of Monte-Carlo trials was anticipated to be relatively small. Using a value of the distortion magnitude, δ_{max}, of 0.125 Å, numerical studies showed that the mean converged after 125 Monte-Carlo trials while the change in the standard deviation between 1000 and 2000 trials was on the order of 2.3%. Therefore, it was deemed adequate to limit each simulation to 1000 Monte-Carlo trials.

Fig. 10 shows skyline representations of typical relative frequency histograms of predicted G_{23} and K_{23} moduli, computed at $\delta_{max} = 0.125$ Å. Both the G_{23} and K_{23} predictions show a skewed distribution about the sample mode, or modulus exhibiting the highest frequency. Because the distortions imposed on the unit cell are uniformly random, there is an equal probability of nanotubes being set closer or further apart. The resulting distributions reflect the fact that the Lennard–Jones

potential yields a higher potential energy consequence for the interaction of more proximal nanotubes under applied strain modes. The shape of the relative frequency histograms suggests a shifted Gamma distribution to provide an approximate probability density function to fit the data.

The probability density function, $h(x)$, for a shifted Gamma distribution is given by

$$h(x) = H(x - \xi)\frac{1}{\Gamma(\alpha)\theta^\alpha}(x - \xi)^{\alpha-1}\exp[-(x - \xi)/\theta]$$
$$0 < x < \infty \tag{3}$$

where ξ is the shift factor, $\Gamma(\alpha)$ and $H(x-\xi)$ are Gamma and Heaviside functions, respectively, and α and θ are fitting parameters. The mean and standard deviation are related to the fitting parameters in the gamma distribution as

$$\mu = \alpha\theta + \xi \quad \text{and} \quad \sigma = \theta\sqrt{\alpha} \tag{4}$$

The fitting parameters were determined by matching as closely as possible the mean value and observed standard deviation of the moduli distributions. The shift and fitting parameters for the transverse shear and bulk moduli are listed in Table 1.

Using the fitting parameters, the mean and standard deviation were computed using the relationships given in Eq. (4). These values are listed in Table 2.

Comparing the results from the Monte-Carlo trials, the mean value of the transverse shear modulus exhibited a drift that varied from 22.5 to 25.8 GPa. The standard deviation, however, demonstrated a high sensitivity to increasing lattice distortion. For a value of δ_{max} equal to 0.175 Å (approximately 1.39% of the center-to-center nanotube separation distance), a single standard deviation increased from zero (perfect lattice) to 3.96 GPa, or 17.6% of the mean G_{23} modulus. The Gamma distribution of G_{23} as a function of the maximum lattice distortion parameter normalized by the equilibrium center-to-center distance is shown in Fig. 11.

A similar set of Monte-Carlo simulations was performed to assess the variation of the transverse bulk modulus, K_{23}, with increasing distortion. In the Monte-Carlo trials, the
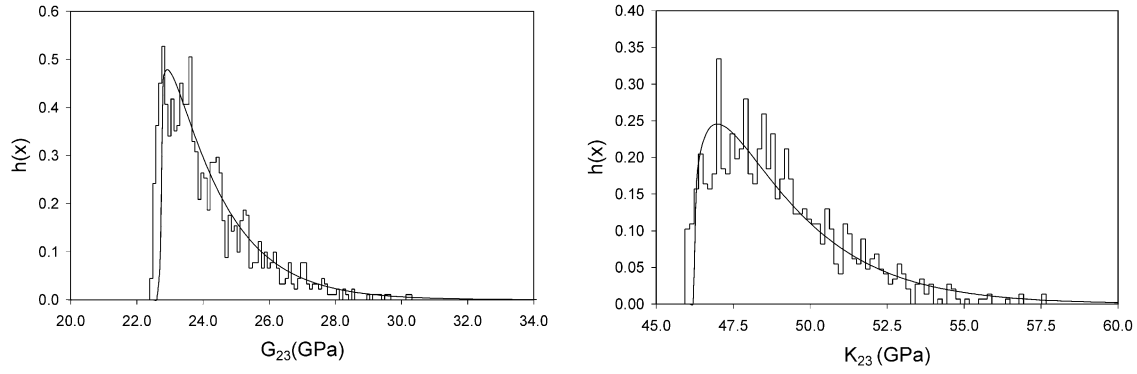
Fig. 10. Relative frequency histograms of predicted G_{23} and K_{23} moduli for $\delta_{max} = 0.125$ Å.

Table 1
Fitting parameters and shift factors for a gamma distribution of elastic moduli for various magnitudes of applied lattice distortion

δ_{max} (Å)	Transverse shear modulus, G_{23}			Transverse bulk modulus, K_{23}		
	α	θ (Å)	ξ (Å)	α	θ (Å)	ξ (Å)
0.0000	0.00	0.00	22.50	0.00	0.00	45.80
0.0625	1.35	0.25	22.54	1.60	0.38	45.99
0.0750	1.55	0.35	22.56	2.30	0.43	45.91
0.0875	1.77	0.43	22.52	2.70	0.50	45.95
0.1000	1.85	0.55	22.48	3.20	0.63	45.78
0.1125	2.20	0.65	22.37	3.70	0.78	45.41
0.1250	2.45	0.77	22.21	3.93	0.93	45.25
0.1375	2.60	0.89	22.18	4.37	1.15	44.57
0.1500	2.90	1.05	21.80	4.70	1.30	44.19
0.1625	3.15	1.24	21.39	5.20	1.50	43.40
0.1750	3.35	1.40	21.10	5.70	1.65	42.70

Table 2
Mean and standard deviation of a gamma distribution obtained from fitting parameters

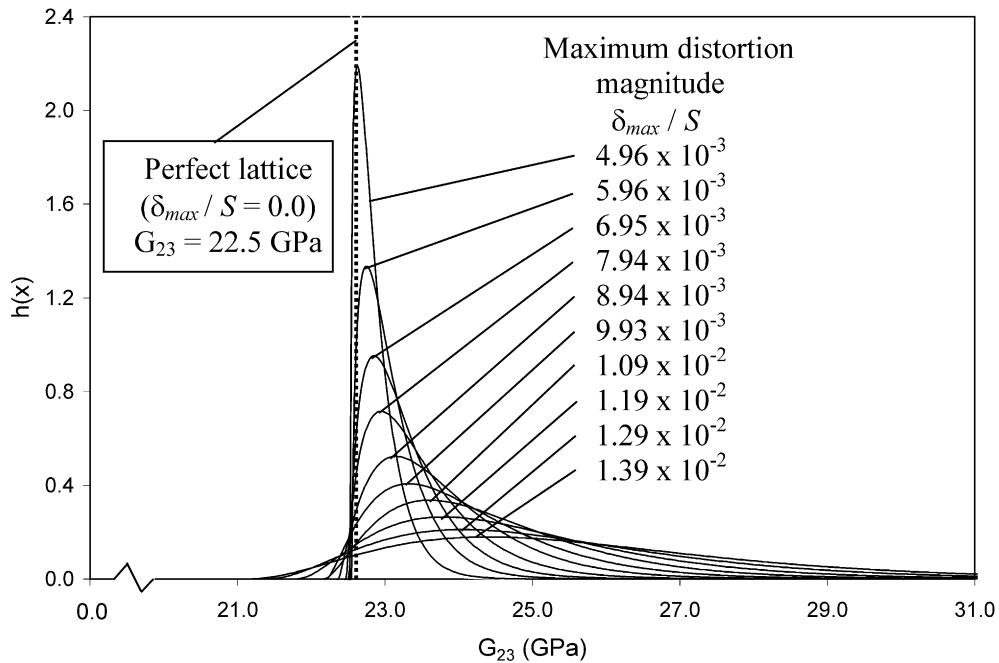| δ_{max} (Å)	Transverse shear modulus, G_{23}		Transverse bulk modulus, K_{23}	
	μ (GPa)	σ (GPa)	μ (GPa)	σ (GPa)
0.0000	22.5	0.00	45.8	0.00
0.0625	22.9	0.68	46.6	0.99
0.0750	23.1	0.92	46.9	1.51
0.0875	23.3	1.16	47.3	1.91
0.1000	23.5	1.37	47.8	2.54
0.1125	23.8	1.77	48.3	3.27
0.1250	24.1	2.15	48.9	3.79
0.1375	24.5	2.45	49.6	4.69
0.1500	24.9	2.97	50.3	5.36
0.1625	25.3	3.51	51.2	6.37
0.1750	25.8	3.96	52.1	7.32

Fig. 11. Normal distributions of G_{23} shear modulus with lattice distortion.
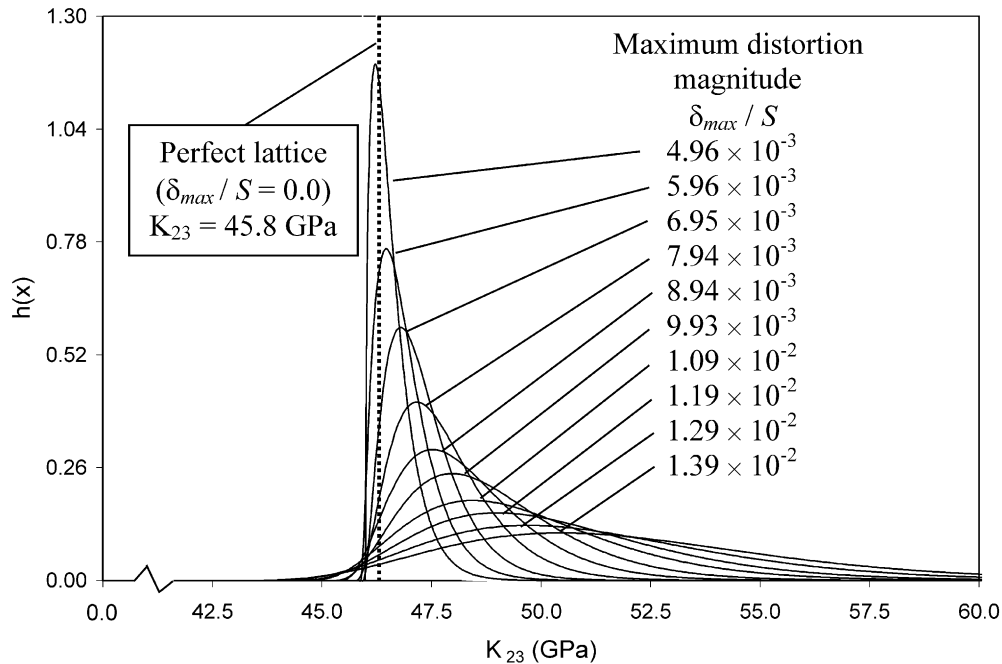
Fig. 12. Normal distributions of K_{23} shear modulus with lattice distortion.

expectation value for the modulus demonstrated a significant drift that varied from 45.8 to 52.1 GPa. For δ_{max} equal to 0.175 Å, a single standard deviation (7.32 GPa) equals 14.1% of the mean K_{23} modulus. The Gamma distribution of K_{23} as a function of the normalized lattice distortion parameter is shown in Fig. 12.

As shown in Figs. 11 and 12 both the bulk modulus, K_{23}, and shear modulus, G_{23}, show a drift in the mean value of the modulus that increases with δ_{max}. This increase can be attributed to the effect of greater nanotube interaction under applied strain modes due to the random distortion or, interpreted differently, the consequential increase in pressure exerted on the nanotubes due to the constant volume constraint used in the present analysis. The principal result for each set of distributions is the large increase in variation with increasing lattice distortion. For structural applications of nanotube bundles—such as microfilamentary hierarchical aggregates of nanotubes as postulated in Fig. 2—distortion sensitivity under combined transverse dilatational and shear straining may contribute to an unacceptably large uncertainty in mechanical properties.

6. Concluding remarks

The transverse moduli of carbon nanotube crystals have been shown to be highly sensitive to small distortions in the packing configuration exhibited by carbon nanotube bundles. This sensitivity is due to the weak and highly nonlinear van der Waals forces that constitute internanotube cohesion, and creates significant uncertainty in the predicted transverse moduli. The intrinsic variation of mechanical properties due to internal faults has important consequences on material integrity and indicates that the development of new synthesis and fabrication methods should maximize the precision in forming nanotube bundle aggregates to mitigate this effect. Alternatively, the present analysis suggests that future research into nanotube bundle synthesis be directed towards functionalization of nanotubes to create covalent cross-links in order to improve cohesion. Improved transverse properties may be required to fully realize the tremendous stiffness and strength potential of carbon nanotube crystals for successful structural applications such as reinforcement in future polymeric composite materials.

References

[1] Hernandez E, Goze C, Bernier P, Rubio A. Elastic properties of C and $B_xC_yN_z$ composite nanotubes. Phys Rev Lett 1998;80: 4502–5.

[2] Salvetat JP, Briggs GAD, Bonard JM, Bacsa RR, Kulik AJ, Stockli T, et al. Elastic and shear moduli of single-walled carbon nanotubes. Phys Rev Lett 1999;82:944–7.

[3] Stone AJ, Wales DJ. Theoretical studies of icosahedral C_{60} and some related species. Chem Phys Lett 1986;128:501–3.

[4] Thess A, Lee R, Nikolaev P, Dai H, Petit P, Robert J, et al. Crystalline ropes of metallic carbon nanotubes. Science 1996;273: 483–7.

[5] Pipes RB, Hubert P. Helical carbon nanotube arrays: mechanical properties. Comp Science Technol 2002;62:419–28.

[6] Saether E, Frankland SJV, Pipes RB. Transverse mechanical properties of single-walled carbon nanotube crystals. Part I: determination of elastic moduli. Comp. Sci. Technol. [in press].

[7] Allen MP, Tildesley DJ. Computer simulation of liquids. Clarendon Press; 1987.

[8] Moore WJ. Physical chemistry. 4th ed. Englewood Cliffs (NJ): Prentice Hall; 1972. p. 913–5.

[9] Green JF, Spain IL. The theory of c-axis elastic moduli of graphite and their strain dependence using simple models of the interplanar interaction. J Phys Chem Solids 1973;34:2177–91.

[10] Green JF, Bolland TK, Bolland JW. Lennard-Jones interaction for hexagonal layered crystals. J Phys Chem Solids 1974;61:1637–46.

[11] Popov VN, Van Doren VE, Balkanski M. Elastic properties of crystals of single-walled carbon nanotubes. Solid State Commun 2000;114:395–9.

[12] Tersoff J, Ruoff RS. Structural properties of a carbon-nanotube crystal. Phys Rev Lett 1994;73:676–9.

[13] Lu JP, Yang W. The shape of large single- and multiple-shell fullerenes. Phys Rev B 1994;49:11421–4.